Septins throughout phylogeny are predicted to have a transmembrane domain, which in *Caenorhabditis elegans* is functionally important.

Jenna A. Perry, Michael E. Werner, Bryan W. Heck, Paul S. Maddox, Amy Shaub Maddox

Department of Biology, University of North Carolina at Chapel Hill, Chapel Hill, NC

Correspondence:

Emails of authors:

jenna_perry@unc.edu

wernerm@email.unc.edu

bwheck@email.unc.edu

pmaddox@email.unc.edu

asm@unc.edu

DATA AVAILABILITY STATEMENT: The data from this study are available from the corresponding author upon request.

FUNDING STATEMENT: Maddox Laboratory is supported by NIGMS of the National Institutes of Health under award numbers **1R35GM144238-01** and the National Science Foundation under award number **2153790.** JAP is also supported by NIH Ruth L. Kirschstein Postdoctoral Individual National Research Service Award through NIGMS under award number **1F32GM143910-01.** This publication is solely the responsibility of the authors and does not reflect the official views of the National Institutes of Health or the National Science Foundation.

CONFLICT OF INTEREST DISCLOSURE: Not applicable

ETHICS APPROVAL STATEMENT: Not applicable

PATIENT CONSENT STATEMENT: Not applicable

PERMISSION TO REPRODUCE MATERIAL FROM OTHER SOURCES: Not applicable

CLINICAL TRIAL REGISTRATION: Not applicable

SUMMARY:

Septins, a conserved family of filament-forming proteins, contribute to eukaryotic cell division, polarity, and membrane trafficking. Septins are thought to act in these processes by scaffolding other proteins to the plasma membrane. The mechanisms by which septins associate with the plasma membrane are not well understood but can involve two polybasic domains and/or an amphipathic helix. We discovered that the genomes of organisms throughout phylogeny, but not most commonly used model organisms, encode one or more septins predicted to have transmembrane domains. The nematode *Caenorhabditis elegans*, which was thought to express only two septin proteins, UNC-59 and UNC-61, translates multiple isoforms of UNC-61, and one isoform, UNC-61a, is predicted to contain a transmembrane domain. UNC-61a localizes specifically to the apical membrane of the *C. elegans* vulva and is important for maintaining vulval morphology. UNC-61a partially compensates for the loss of the other two UNC-61 isoforms, UNC-61b and UNC-61c. The UNC-61a transmembrane domain is sufficient to localize a fluorophore to membranes in mammalian cells, and its deletion from UNC-61a recapitulates the phenotypes of *unc-61a* null animals. The localization and loss-of-function phenotypes of UNC-61a and its transmembrane domain suggest roles in cell polarity and secretion and help explain the cellular and tissue biological underpinnings of *C. elegans* septin null alleles' enigmatically hypomorphic phenotypes. Together, our findings reveal a novel mechanism of septin-membrane association with profound implications for the dynamics and regulation of this association.

KEYWORDS:

Septins, *C. elegans*, transmembrane domain, cytoskeleton

INTRODUCTION :

Septins comprise a family of filamentous GTPases that are conserved in most eukaryotes but absent in land plants [1,2]. Based on protein sequence homology, septins can be grouped into 5 classes – Groups 1 & 2 are found in animals and fungi, Groups 3-4 are only found in fungi, and Group 5, which are thought to be ancestral [1–5]. Septins within Groups 1-4 form non-polar heterooligomers, which through association with the plasma membrane, polymerize into filaments and other higher-order structures like meshes and rings [6–10]. Septins scaffold regulatory and cytoskeletal proteins involved in many cellular functions including division, adhesion, and polarization [11,12].

Septin proteins have evolutionarily variable N- and C- terminal extensions that flank a conserved GTP-binding domain and septin unique element. Three septin motifs have been implicated in facilitating membrane association: polybasic region 1 (PB1), polybasic region 2 (PB2), and the amphipathic helix (AH)[1,13–16]. Both PB1, located at the N-terminus of the GTP-binding domain, and PB2, located toward the C-terminus of the GTP-binding domain, can confer the specificity of lipid binding *in vitro* [15–18]. The AH domain, which is found in some C-terminal coiled-coils, detects and binds to lipid packing defects within curved membranes to facilitate micron-scale curvature sensing [14,19]. While these domains help septins associate with membranes, they are not sufficient for membrane interaction [13–16,18]. Some unicellular organisms including *Tetrahymena thermophila* and *Chlamydomonas reinhartii* have been reported to have septins containing putative transmembrane domains, but the requirement and roles of these domains have not been tested and transmembrane domains in animal septins are not known to exist [4,20].

The study of septins in many organisms, including unicellular model organisms like budding yeast, is complicated by the large number (5+) of septin genes, and often splice isoforms [2,21]. In contrast, the *C. elegans* genome encodes two septin genes, *unc-59* and *unc-61***,** that in turn produce a total of four protein products: UNC-59, UNC-61a (the TMD-septin), UNC-61b, and UNC-61c. Although *C. elegans* contains a reduced cohort of septins as compared to other model organisms, the *C. elegans* septins are homologous to the core septins of other animals and fungi, and can form nonpolar filaments from palindromic tetramers [2,22,23]. The *C. elegans* septins localize similarly to core septins in other organisms, including to the cytokinetic ring [23,24]. Loss of septin function results in several phenotypes, including uncoordinated movement, germline extrusion, and vulval protrusion, that occur in well studied tissues, like the vulva, but the role of septins in these tissues remains unclear [23,25,26].

Here, we report the presence of putative transmembrane domain (TMD)-containing septins throughout phylogeny. To validate the expression and functionality of a TMD-septin, we used the nematode *Caenorhabditis elegans* as a model. UNC-61a, the TMD-containing septin, has a unique localization pattern as compared to UNC-61b and UNC-61c, yet UNC-61a can partially rescue the effects of loss of UNC-61b and UNC-61c on animal motility and vulval morphogenesis. To demonstrate TMD functionality, we used two approaches: 1) introduce a transgene containing StayGold GFP fused to only the *C. elegans* TMD sequence and 2) deletion of the TMD from UNC-61a in *C. elegans.* In mammalian cells, the TMD::StayGold GFP was sufficient to interact with membranes. In *C. elegans* animals lacking the TMD from UNC-61a (UNC-61a ΔTMD) recapitulated the post-embryonic developmental phenotypes of *unc-61a* null animals. Loss of the TMD led to abnormally open vulval membranes and to detachment of surrounding tissues from the cuticle. The presence of a functional TMD septin, together with the presence of putative TMD-septins throughout phylogeny, suggests that transmembrane domains, and thus highly stable interactions, couple septins to membranes.

MATERIALS AND METHODS:

Phylogenetics: To find transmembrane domain (TMD) containing septins, we searched UniProt[27] using accession code IPR030379 to identify putative septins based on the presence of a Septin-type guanine nucleotide-binding (G) domain. Then, the resultant list was filtered for the "Transmembrane" annotation in UniProt. This filter uses the SAM (Sequence Analysis Methods) for automatic annotation to predict putative transmembrane domain when there is an overlap of at least 10 amino acids between TMHMM and Phobius predictors [28,29]. The filtered list hits were parsed for duplicates, then organisms containing TMD-septins were plotted on a phylogenetic tree using Interactive Tree of Life (iTOL)[30]. TMD-septins from selected model organisms were validated using DeepTMHMM[31], a deep learning transmembrane domain predictor. The location of the TMD was assessed using UniProt and septin group homology was determined using SHOOT[32]. Protein

sequence alignments were conducted using MUSCLE[33] in MEGA11[34]. A neighbor-joining tree was generated with 100 bootstrap replicates for statistical support in MEGA11.

C. elegans strains and culture: *C. elegans* strains were maintained at 20 °C using standard culturing conditions [35]. The strains used and/or generated for this work are listed in the table below.

Strain	Genotype	Phenotype	Source or Reference
COP2586	knuSi921[pNU3401(AMAD02-unc-61p::UNC-61(a)::GFP-C1::unc-61u+, unc-119(+))] II; unc-119(ed3)III.	UNC-61a::GFP-C1	InVivo Biosciences/This work
NK2228	unc-59(qy50 [unc-59::GFP-C1:;3xflag::AID]) I.	UNC-59::GFP-C1	Chen *et al.*
MDX130	unc-59(qy50 [unc-59::GFP-C1:;3xflag::AID]) I; unc-61a(mon24 [unc-61a S2X]) V	UNC-59::GFP-C1; UNC-61a null	This work
MDX118	unc-61(mon22 [unc-61 KO]) V.	UNC-61 KO	This work
MDX138	knuSi921[pNU3401(AMAD02-unc-61p::UNC-61(a)::GFP-C1::unc-61u+, unc-119(+))] II; unc-119(ed3)III ; unc-61(mon22 [unc-61 KO]) V.	UNC-61a::GFP-C1; UNC-61 KO	This work
MDX140	knuSi921[pNU3401(AMAD02-unc-61p::UNC-61(a)::GFP-C1::unc-61u+, unc-119(+))] II; unc-119(ed3)III; unc-61a(mon24 [unc-61a S2X]) V	UNC-61a::GFP-C1; UNC-61a null	This work
MDX132	unc-59(qy50 [unc-59::GFP-c1:;3xflag::AID]) I; unc-61a(mon26 [unc-61a L7_V29del]) V.	UNC-59::GFP-C1; UNC-61a TM del	This work
LP193	cpIS56[Pmex-5::TAGRFPT:: PLCδ-PH::tbb-2 3'UTR + unc-119 (+)] II; unc-119(ed3) III.	Red GL Membrane	CGC
FT1197	xnls449[lin-26::lifeAct::GFP + unc-119(+)].	Actin::GFP	CGC
MDX150	unc-61a(mon26 [unc-61a L7_V29del]) V; xnls449[lin-26::lifeAct::GFP + unc-119(+)].	UNC-61a ΔTMD; Actin::GFP	This work
COP2601	knuSi934 [pNU3400 (AMAD01- unc-61p:: wrmScarlet::UNC-61(B/C)::unc-61u, unc-119(+))] II; unc-119(ed)III.	wrmScarlet ::UNC-61b/c	InVivo Biosciences/ This work
MDX152	knuSi934 [pNU3400 (AMAD01- unc-61p:: wrmScarlet::UNC-61(B/C):: unc-61u, unc-119(+))] II; unc-119(ed)III; unc-61a (mon26 [unc-61a L7_V29del]) V.	wrmScarlet ::UNC-61b/c; UNC-61a ΔTMD	This work

Human cell culture: HeLa cells were maintained at 37°C in DMEM with 10% Fetalplex and 1% Pen/Strep.

Fluorescence imaging conditions and analysis:

***C. elegans*:** C. elegans fluorescence imaging was performed as previously described [25]. Whole worm images were acquired using a Nikon A1R microscope with a 60 × 1.27 NA Nikon water immersion objective with a gallium arsenide phosphide photo-multiplier tube (GaAsP PMT) using NIS-Elements software. 25-30 confocal sections were acquired with 1 µm z-spacing.

HeLa cells: Cells were grown in a 35 mm glass bottom dish (81158, Ibidi), transfected with transgenes (see below), and fixed with 4% PFS in PBS for 15 minutes. Prior to staining, cells were permeabilized and blocked in PBS+0.1% Triton-X100 (PBST) containing 5% Normal Donkey Serum for 1 hr at room temperature. Primary antibody (Rabbit α GM130, 1:2500, Cell Signaling 12480) was diluted in blocked buffer and incubated with the cells for 1 hr at room temperature. Counterstains (DAPI; 647-Phalloidin, Cell Signaling 8940) were diluted with the secondary antibody (560 nm α rabbit) in blocking buffer and incubated for 1 hr at room temperature. Cells were imaged using a Nikon A1R microscope with a 100 × 1.35 NA Nikon silicone immersion objective with a with a gallium arsenide phosphide photo-multiplier tube (GaAsP PMT) using NIS-Elements software. 10-15 confocal sections were acquired with 1.5 µm z-spacing.

C. elegans CRISPR/Cas9 genome editing and sequencing: CRISPR/Cas9 was performed as previously described[36]. Briefly, a mix containing crRNA, tracrRNA, and Cas9 protein with a *dpy-10* co-CRISPR was injected into the gonad of young adult animals. Benchling electronic lab notebook [37] was used to select the best Cas9 cleavage site, and the best sequence for the crRNAs, along with off-target predictions. The edited locus was amplified via PCR from *C. elegans* genomic DNA extracted from 8-10 adult worms using the Extract-N-Amp™ Tissue PCR Kit (Millipore Sigma, MA) as previously described[38] then sequenced. The resultant worm strains were outcrossed to N2 control animals.

CRISPR/cas9 Targeting Sequences

Gene	Targeting Sequence
unc-61	ttttttattcgaactcgatg ; tcttaacttctttgacactt
unc-61a	ttttttattcgaactcgatg
unc-61a transmembrane domain	ttttttattcgaactcgatg ; ccgcttttctcatcgtccga

CRISPR/cas9 Repair Sequences

Gene	Repair Sequence
unc-61a null	*ActctgctgaccagacgatttttattcgaactcgatgagAagcacaactgacgaatcgatagataatttATGtAGTTTC GAAACGATTCTCTATACTGCATCTGCCCTTCTT*
unc-61a transmembrane domain deletion	*actctgctgaccagacgatttttattcgaactcgatgagTagcacaactgacgaatcgatagataatttATGAGTTTCG AAACGATTCGACGATCGAAACAAAGCAGCATAAACCTGCAGAC*

Primer sequences

Primer	Sequence
UNC-61 null 5' PCR Primer	gacagttgttggttatatttgc
UNC-61 null 3' PCR Primer	tgggtgtagtgtgtatttgaaa
UNC-61a deletion 5' PCR Primer	ccgcttttctcatcgtccga
UNC-61a deletion 3' PCR Primer	gctgcaattgttggcttcttgc
UNC-61a transmembrane domain deletion 5' PCR Primer	ccgcttttctcatcgtccga
UNC-61a transmembrane domain deletion 3' PCR Primer	gctgcaattgttggcttcttgc

Mammalian plasmid construction and stable cell lines: Transgenes were cloned into a backbone containing a CAG promoter, IRES, and hygromycin resistance cassette – all flanked by PiggyBac inverted repeats. Cell lines were each generated by co-transfecting HeLa cells with the respective expression plasmid and a vector containing the PiggyBac transposase (PB210PA-1, Systems Biosciences), and then selected with Hygromycin B (200ug/ml). HeLa cells were maintained at 37°C in DMEM (10% Fetalplex, 1% Pen/Strep), and transfections were performed with Effectene (301425, QIAGEN) according to the manufacturer's instructions.

Brood size: L4-staged animals were selected from a non-starved growth plate and placed on individual culture plates at 20 °C for 48 hours, after which the adult animal was removed. After two days, the plates with larval offspring were moved to 4 °C for 20 minutes to halt worm movement. All larvae and unhatched embryos were manually counted using a clicker on a Nikon SMZ800 dissection microscope.

Plate level phenotype analysis: To score plate-level phenotypes, a single L4 animal was transferred to a culture plate and allowed to lay embryos for 48 hours, after which the adult was removed. After 3 days, when the progeny became adults, the plate-level phenotypes were manually assessed and scored using a Nikon SMZ800 dissection microscope.

Thrashing assay: Animal motility was scored via thrashing in M9 buffer (22 mM KH_2PO_4, 42 mM Na_2HPO_4, 85 mM NaCl, 1 mM $MgSO_4$). To perform the thrashing assay, L4 animals were first transferred for 5 minutes to an unseeded culture plate

to remove any food adhered to their body. The animals were then transferred to 15 µl of M9 buffer on a 15-well multitest slide and allowed to acclimate for 1 minute. Animals were then imaged for 30 seconds using a Moticam X camera (Motic, California, US) mounted to the eyepiece of a Nikon SMZ800 dissection microscope and recorded using a Samsung Galaxy S10 mobile device. Movies were converted from MP4s to AVIs using FFMPEG. To calculate thrashing frequency, body thrashes per 30 seconds were counted for at least 10 animals per genotype.

Plate motility assay: Animal movement on seeded NGM plates was scored by measuring total track length. To perform the assay, L4 animals were transferred to the center of a seeded NGM plate and allowed to explore for 10 minutes. After 10 minutes, the plates were imaged using the Pro camera setting with 2.8x zoom on a Samsung Galaxy S10 mobile device. Track length was quantified using the freehand line tool in Fiji[39]. A total of 30 animals per condition were analyzed.

Figures and statistical analysis: Image vignettes were made from images cropped in Adobe Photoshop and assembled in Adobe Illustrator. GraphPad Prism software was utilized to generate graphs and perform appropriate statistical analysis. In short, an analysis of variance (ANOVA) corrected with Tukey Multiple Comparison test determined statistical significance for all figures. Assumptions for normality and equal variance were made for all analyzed data. A *p* value less than 0.05 was considered significant. All figures report significance testing results and standard deviation error bars. All legends and figures include sample size (*n)* and *p* value.

RESULTS:

Septins throughout phylogeny contain putative transmembrane domains

To explore the presence and identity of conserved motifs in septins throughout opisthokont and non-opisthokont lineages, such as those that confer septin-membrane association, we performed a bioinformatic survey using Uniprot [27]. Our survey revealed the presence of sequences encoding putative transmembrane domain (TMD) in septin genes from many organisms across phylogeny (Figure 1A). Out of roughly 34,000 protein sequences annotated as Septin-type guanine nucleotide-binding (G) domain containing proteins (IPR030379), 686 (~2%) contained predicted TMDs. Remarkably, putative TMD-containing septins ("TMD-septins") are not restricted to specific clades but can be found throughout the tree of life. Of the 2320 eukaryotic species predicted to express septin-like proteins, 447, or nearly 20%, possess at least one TMD-septin. TMD-septins were absent from many well-established model organisms including budding yeast, fruit fly, and mouse, but present in several others including the nematode *Caenorhabditis elegans* (Figure 1B). We used a deep learning model for transmembrane topology prediction and classification (Deep TMHMM) to quantify the prediction of a TMD-septin in *C. elegans*; amino acids 5-29 are predicted, with 99-100% certainty, to form a TMD (Figure 1C). Alignment of homologous septin sequences from several nematode species revealed that although the *C. elegans* septin diverged from other nematode species, a putative TMD-septin was well-conserved in nematodes (Figure 1D). Taken together, these data suggest that TMDs may be a more widespread feature of some septins than previously appreciated, and that a *C. elegans* septin contains a predicted TMD.

C. elegans septin UNC-61a contains a putative transmembrane domain and is differentially localized compared to UNC-61b/c and UNC-59

Most commonly used model organisms, including unicellular organisms such as budding yeast, have a complex septin collection, with five or more septin genes, and in many organisms, septin genes can furthermore have multiple splice isoforms. *C. elegans* has a uniquely simple set of septins, with two septin genes, *unc-59* and *unc-61*, that are homologous to human SEPT7 and SEPT6/8 [2]. UNC-59 and UNC-61 proteins together form palindromic tetramers *in vitro* with two UNC-61 proteins in the center and UNC-59 on each end [22]. These two septins exhibit behaviors shared by other organisms' septins, including enrichment in and requirement for normal function of the cytokinetic ring [22,23,39–41] . Loss of septin function in *C. elegans* also leads to morphological defects of the *C. elegans* syncytial germline and reduced fertility [23–26]. While the *C. elegans* septins have been considered as a two-protein system, in fact, one of the *C. elegans* septin genes, *unc-61*, encodes three isoforms: a, b, and c (Figure 2A). *unc-61b* and *unc-61c* are splice isoforms encoding proteins that

differ only by a single stretch of four amino acids, a distinction that we do not interrogate here; hereafter we refer to UNC-61b and UNC-61c collectively as UNC-61b/c. *unc-61a* is transcribed from an alternative start site upstream of the *unc-61b/c* start codon. Much of the domain organization of UNC-61a is nearly identical to that of UNC-61b/c, with a conserved GTP-binding domain and a C-terminal extension containing a coiled-coil and amphipathic helix. Uniquely, UNC-61a has a longer N-terminal extension that contains the predicted transmembrane domain (Figure 2B). Previous localization and loss-of-function studies of UNC-61 did not differentiate among UNC-61a and UNC-61b/c. [23,26].

To detect UNC-61a expression and compare its localization to that of UNC-61b/c and UNC-59, we generated animals expressing an internally-GFP tagged UNC-61a under the control of the *unc-61a* promoter at a Mos1-mediated single copy insertion (MosSCI) site (Figure 2C)**.** A similar MosSCI approach was utilized to create an N-terminal wrmScarlet-labeled UNC-61b/c (wrmScarlet::*unc-61b/c;* Figure 2C). UNC-61a::GFP strongly localized to the pharynx and vulva in adult animals, while wrmScarlet::UNC-61b/c was weakly expressed in those structures (Figure 2D). Conversely, wrmScarlet::UNC-61b/c was strongly expressed in the *C. elegans* germline (Figure 2D). Interestingly, UNC-59::GFP localization pattern is an amalgamation of the UNC-61a and UNC-61b/c localization patterns: present in pharynx, germline, and vulva (Figure 2D). The differential localization patterns of the UNC-61 isoforms suggest that the isoforms mediate distinct biological processes in the tissues that they are expressed. Furthermore, UNC-59 may function with both UNC-61a and UNC-61b/c, in different tissues.

UNC-61a partially rescues the loss of UNC-61b/c

Given the unique protein domain structure of UNC-61a, we next examined what functions previously assigned to UNC-61a/b/c, collectively, specifically require UNC-61a. First, since UNC-61 localizes to the oogenic germline, we tested whether loss of UNC-61a perturbed animal fecundity. We generated animals that contained an *unc-61a* null allele created through the introduction of a stop codon after the alternative start codon of *unc-61a* at the endogenous locus to maintain the expression of UNC-61b/c (Figure 3A). We assessed the fecundity of *unc-61a* null animals by placing individual fourth-larval stage (L4) animals onto culture plates for 48 hours. After allowing the founder animals' progeny to develop for another 48 hours, larvae and unhatched embryos were counted. As expected from GFP-tagged UNC-61a being undetectable in the germline, loss of UNC-61a expression did not reduce fecundity compared to controls (Figure 3B).

While assessing fecundity via stereoscope, we noticed that *unc-61a* null animals had adult phenotypes frequently associated with septin loss-of-function [23,25]. We quantified the penetrance of phenotypes associated with vulval tissue biogenesis, morphogenesis, and/or function. We scored animals early in the adult stage for the presence and severity of protruded vulvas (pvl) and for embryos older than expected in the uterus indicating an egg-laying defect (egl). As compared to control animals, roughly 45% of *unc-61a* null animals had slightly protruded vulvas and a small percentage (5%) had an egg-laying defect (Figure 3C). Thus, UNC-61a influences the morphogenesis and function of the vulva, but not of the germline.

We next tested whether exogenous UNC-61a could compensate for the loss of UNC-61a expression from the endogenous locus. Animals expressing GFP-tagged UNC-61a from the MosSCI locus with the *unc-61a* null allele at the endogenous locus, did not have protruded vulvas nor showed signs of an egg-laying defect (Figure 3D). This indicates that the exogenously expressed, fluorescently tagged UNC-61a can replace endogenous UNC-61.

Finally, we examined for what UNC-61a/b/c functions UNC-61a is sufficient. To this end, we first generated animals containing an endogenous deletion of the entire *unc-61* locus, to eliminate all three transcripts. This UNC-61 null animal served as the genetic background where we created an animal that solely expressed UNC-61a::GFP from the MosSCI locus (Figure 3E). We then assessed the fecundity of these animals compared to control and UNC-61 null animals. As expected, control animals and animals expressing UNC-61a::GFP in the presence of endogenous UNC-61 had similar size broods, however the broods of UNC-61 null animals and animals expressing only UNC-61a were significantly smaller (approximately 6% and 10% the size of control, respectively (Figure 3F). The broods of UNC-61 null animals and UNC-61a only animals were not significantly different than each other (Figure 3F) suggesting that UNC-61a is not sufficient to rescue germline phenotypes caused by loss of endogenous UNC-61.

Although expression of only UNC-61a did not rescue loss of endogenous UNC-61 in the germline, these animals did show a reduced penetrance of plate-level phenotypes cause by UNC-61 loss-of-function. Interestingly, animals expressing only UNC-61a had less severe vulval protrusion (pvl) phenotypes than UNC-61 null animals (approximately 55% slight pvl vs 20% slight pvl, respectively), along with reduced incidence of egg-laying defects (Figure 3G). Overall, these results suggest that UNC-61a can partially rescue vulval phenotypes related to loss of endogenous UNC-61.

Another hallmark of septin loss of function in *C. elegans* is uncoordinated movement [26,35,43,44]. To understand if expression of UNC-61a alone could restore *C. elegans* motility, we imaged animals in liquid medium to measure thrashing, counting the number of body bends as a function of time. Loss of endogenous UNC-61 caused a reduction in thrashing, which was not rescued by expression of UNC-61a (Figure 3H). By contrast, motility on solid media (crawling) was higher in animals expressing only UNC-61a than for animals lacking all isoforms of UNC-61 (Figure 3I). This suggests that UNC-61a is sufficient to partially rescue the uncoordinated movement phenotype associated with loss of UNC-61 function. Taken together, these results demonstrate that UNC-61a is functionally important and that it contributes to tissue morphogenesis and function independent of the other UNC-61 isoforms.

UNC-61a transmembrane domain is sufficient to drive localization to cellular membranes.

Given that UNC-61a differs from UNC-61b/c by its N-terminal extension, we next tested how these residues directed the localization of GFP *in vivo*. To this end, we created a mammalian expression construct containing the entire N-terminal extension unique to UNC-61a (the first 71 amino acid residues; V1). We co-labeled these cells with phalloidin to visualize F-actin, Hoescht for DNA, and anti-GM130, a cis-Golgi marker, to gain a better understanding of our V1::StayGold GFP localization (Figure 4A). V1::StayGold GFP localized proximal to the GM-130 signal, suggesting that these residues of C. elegans UNC-61a are sufficient to confer localization to intracellular membranes.

Since the only predicted structural domain unique to the UNC-61a N-terminal extension is its TMD, we created a smaller construct (V2) that included only the first 48 amino acid residues, where residues 5-29 encode the TMD, of UNC-61a. V2::StayGold GFP localized to the nuclear envelope (Figure 4B). These findings demonstrate that the predicted TMD of a *C. elegans* septin is sufficient for membrane localization and therefore direct association.

Loss of UNC-61a TMD disrupts vulval morphology.

To determine the importance of the UNC-61a TMD, we next tested the extent to which *unc-61a* null phenotypes result from the absence of the TMD. To do so, we removed only the sequence encoding the TMD from the endogenous locus of *unc-61* using CRISPR/Cas9 (Figure 5A). Loss of the TMD phenocopied the loss of UNC-61a, with no discernable effect on animal fecundity (Figure 5B) and a similar penetrance of vulval morphogenesis phenotypes (Figure 5C).

Given the pvl phenotypes in UNC-61a ΔTMD animals, we examined vulval morphology to better understand the roles of the TMD in the vulva. The vulval lumen, through which embryos exit and sperm enter, is lined by the apical surfaces of the vulval epithelial cells [45,46] (Figure 5D). [45–47]. Unless opened by contraction of the associated muscle cells, the vulval lumen remains in a closed conformation [48–50]. In adult animals that express lifeAct::GFP to label F-actin in epidermal cells, the vulva of the UNC-61a ΔTMD animals remained in an open confirmation. Frequently, the surrounding tissue appeared detached from the ventral cuticle (Figure 5E). Together with our observation that UNC-61a specifically localizes to the vulval lumen in adult worms (Figure 2D) these results suggest that UNC-61a contributes to vulval morphology. In sum, our work demonstrates the functional importance of a septin bearing a transmembrane domain.

DISCUSSION AND CONCLUSION:

In this work, we identified the presence of septins containing TMDs in organisms throughout phylogeny and we validated the functionality of the *C. elegans* uncharacterized UNC-61 isoform, UNC-61a, that contains a TMD. We found that UNC-61a is differentially expressed in the apical membrane of the vulva and in the terminal bulb of the pharynx. Loss of UNC-61a resulted in defective vulval morphology. UNC-61a is sufficient to partially rescue phenotypes caused by the loss of the

other UNC-61 isoforms, particularly with respect to vulval morphogenesis and animal motility. Furthermore, we showed that UNC-61a TMD is indeed functional, as tagging it with StayGold GFP expressed in HeLa cells is sufficient to localize the fluorophore to membranes, and excision of the TMD from UNC-61a in *C. elegans* recapitulates the vulval defects associated with the loss of UNC-61a. To our knowledge, our results represent the first evidence for the presence of a validated TMD in any septin that is required for septin function. Our work implicates the TMD in targeting septins to membranes, a novel and evolutionarily conserved mechanism for septin-membrane interaction.

Our search for TMDs in septins throughout phylogeny identified roughly 700 sequences from 450 organisms. While the entirety of this list needs to be validated, our search revealed that within classes, the TMD-septin sporadically appears. Several factors could contribute to the sporadic appearance of TMD-septins throughout phylogeny. Transmembrane predictor programs could have missed TMD sequences that do not match program criteria. Alternatively, the sporadic appearance could reflect sporadic loss during the evolution from an ancestral septin that possessed the TMD. Septins' TMD can occur on either the N- or C-terminus. Given the evolutionary distance among species encoding TMD-septins, this inconsistency is not unprecedented and may indicate exon shuffling, wherein exons that correspond to functional gene domains are duplicated, changed, and rearranged to give rise to proteins with new functions while maintaining[51–53]. Further analysis of the DNA sequence surrounding the TMD will help test whether exon shuffling occured in the evolution of TMD-septins.

To date, three domains (the amphipathic helix (AH) and polybasic domain 1 and 2 (PB1/2)) have been identified to facilitate septin-membrane interactions. AHs sense membrane curvature and PB1/2 confer lipid binding specifity[13,14]. Disruption of these domains, however, is not sufficient to perturb septin localization to cellular membranes[13–18]. This may have been attributed to septins' indirect association with the plasma membrane via other cytoskeletal components such as the scaffold protein anillin that directly binds the plasma membrane[24,54–56]. The presence of a validated TMD sufficient for membrane interaction in a multicellular organism prompts reconsideration of mechanisms through which septins interact with cellular membranes. Until this point, the majority of septin biology has been studied in species that appear not to contain TMD-septins. It remains to be examined whether the septins of a given species or cell type use one or more of the now three mechanisms of membrane association. Validation of TMD-septins in other species will be crucial to understand how septins interact with cellular membranes.

The *C. elegans* TMD-septin UNC-61a localizes to distinct regions of the adult animal: the terminal bulb of the pharynx and the apical membrane of the vulval epithelial cells. Interestingly, a key function of these highly dynamic tissues is to secrete extracellular matrix[49,57]. The vulva may remain open in UNC-61a ΔTMD animals due to a defect in secretion at vulval epithelial cells' apical surface [58–63]. For example, an O-glycan is highly enriched on the vulval lumen and under the flaps of cuticle that flank the vulval slit, in two half-circles where UNC-61a is uniquely enriched[64,65]. Abnormal vulval opening may explain the germline extrusion phenotype of loss of septin function in *C. elegans*[23,25].

While the low expression level of UNC-61a relative to UNC-61b/c led UNC-61a (and by extension the TMD) to be understudied [26], its functionality in *C. elegans* prompts us to rethink the fundamental unit of septin polymerization in this organism. In *C. elegans*, the fundamental septin heteromer is likely not always a tetramer of two copies of UNC-59 and two copies of UNC-61b/c. Rather, UNC-61a may replace UNC-61b/c in some cell types, or UNC-61a may incorporate into a palindromic hexamer in cells where all three polypeptides are expressed. Variability in the stoichiometry of septin oligomers has precedent in human septin heteromers, which can be hexamers or octamers, can co-polymerize into heterogeneous filaments[66]. Similarly, tubulin isotypes with low expression can alter microtubule polymer dynamics, and, in turn, cellular and tissue-level implications such as in cancer prognosis [57,67–70]. We predict that TMD-septins, even when present as minor components of a septin system, can be interspersed into septin filaments and have profound effects on septin functions such as membrane association. Reconstitution of septin collections including TMD-septins, and genetic tuning of septin expression in *C. elegans* will help elucidate biochemical characteristics of TMD-containing filaments and how they function.

ACKNOWLEDGMENTS:

The authors would like to thank the following individuals for fruitful discussions on this work: Lil Fritz-Laylin, Amy Gladfelter, Bob Goldstein, Kacy Gordon, Manos Mavrakis, Michelle Momany, Brent Shuman, and members of the Maddox labs. We would also like to thank Linnea Wethekam for critical reading of this manuscript. Some strains used in this work were provided by the Caenorhabditis Genetic Center (CGC), which is funded by NIH Office of Research Infrastructure Programs (P40 OD010440).

The Maddox Laboratory is supported by a National Institutes of Health award (1R35GM144238-01) and by the National Science Foundation award (2153790) to ASM. This project received funding from the UNC Lineberger Comprehensive Cancer Center via a Discovery Award to ASM. JAP was also supported by a NIH Ruth L. Kirschstein Postdoctoral Individual National Research Service Award (1F32GM143910). This publication is the sole responsibility of the authors and does not reflect the official views of the NIH or NSF.

AUTHOR CONTRIBUTIONS:

Conceptualization, J.A.P; Methodology, J.A.P and M.E.W,; Investigation, J.A.P, M.E.W, and B.W.H; Resources, P.S.M and A.S.M; Writing – Original Draft, J.A.P; Writing – Review & Editing, J.A.P, M.E.W, and A.S.M; Visualization – J.A.P; Supervision, A.S.M; Funding Acquisition, J.A.P and A.S.M

REFERENCES:

1. Pan, F., Malmberg, R.L., and Momany, M. (2007). Analysis of septins across kingdoms reveals orthology and new motifs. BMC Evolutionary Biology *7*, 103. 10.1186/1471-2148-7-103.

2. Shuman, B., and Momany, M. (2022). Septins From Protists to People. Frontiers in Cell and Developmental Biology *9*.

3. Cao, L., Ding, X., Yu, W., Yang, X., Shen, S., and Yu, L. (2007). Phylogenetic and evolutionary analysis of the septin protein family in metazoan. FEBS Letters *581*, 5526–5532. 10.1016/j.febslet.2007.10.032.

4. Nishihama, R., Onishi, M., and Pringle, J.R. (2011). New Insights into the Phylogenetic Distribution and Evolutionary Origins of the Septins. Biol Chem *392*, 681–687. 10.1515/BC.2011.086.

5. Auxier, B., Dee, J., Berbee, M.L., and Momany, M. (2019). Diversity of opisthokont septin proteins reveals structural constraints and conserved motifs. BMC Evolutionary Biology *19*, 4. 10.1186/s12862-018-1297-8.

6. Rodal, A.A., Kozubowski, L., Goode, B.L., Drubin, D.G., and Hartwig, J.H. (2005). Actin and Septin Ultrastructures at the Budding Yeast Cell Cortex. Mol Biol Cell *16*, 372–384. 10.1091/mbc.E04-08-0734.

7. Sirajuddin, M., Farkasovsky, M., Hauer, F., Kühlmann, D., Macara, I.G., Weyand, M., Stark, H., and Wittinghofer, A. (2007). Structural insight into filament formation by mammalian septins. Nature *449*, 311–315. 10.1038/nature06052.

8. Bertin, A., McMurray, M.A., Pierson, J., Thai, L., McDonald, K.L., Zehr, E.A., García, G., Peters, P., Thorner, J., and Nogales, E. (2012). Three-dimensional ultrastructure of the septin filament network in Saccharomyces cerevisiae. MBoC *23*, 423–432. 10.1091/mbc.e11-10-0850.

9. DeMay, B.S., Meseroll, R.A., Occhipinti, P., and Gladfelter, A.S. (2009). Regulation of Distinct Septin Rings in a Single Cell by Elm1p and Gin4p Kinases. Mol Biol Cell *20*, 2311–2326. 10.1091/mbc.E08-12-1169.

10. DeMay, B.S., Bai, X., Howard, L., Occhipinti, P., Meseroll, R.A., Spiliotis, E.T., Oldenbourg, R., and Gladfelter, A.S. (2011). Septin filaments exhibit a dynamic, paired organization that is conserved from yeast to mammals. J Cell Biol *193*, 1065–1081. 10.1083/jcb.201012143.

11. Woods, B.L., and Gladfelter, A.S. (2021). The state of the septin cytoskeleton from assembly to function. Current Opinion in Cell Biology *68*, 105–112. 10.1016/j.ceb.2020.10.007.

12. Marquardt, J., Chen, X., and Bi, E. (2019). Architecture, remodeling, and functions of the septin cytoskeleton. Cytoskeleton *76*, 7–14. 10.1002/cm.21475.

13. Omrane, M., Camara, A.S., Taveneau, C., Benzoubir, N., Tubiana, T., Yu, J., Guérois, R., Samuel, D., Goud, B., Poüs, C., et al. (2019). Septin 9 has Two Polybasic Domains Critical to Septin Filament Assembly and Golgi Integrity. iScience *13*, 138–153. 10.1016/j.isci.2019.02.015.

14. Cannon, K.S., Woods, B.L., Crutchley, J.M., and Gladfelter, A.S. (2019). An amphipathic helix enables septins to sense micrometer-scale membrane curvature. Journal of Cell Biology *218*, 1128–1137. 10.1083/jcb.201807211.

15. Tanaka-Takiguchi, Y., Kinoshita, M., and Takiguchi, K. (2009). Septin-Mediated Uniform Bracing of Phospholipid Membranes. Current Biology *19*, 140–145. 10.1016/j.cub.2008.12.030.

16. Casamayor, A., and Snyder, M. (2003). Molecular Dissection of a Yeast Septin: Distinct Domains Are Required for Septin Interaction, Localization, and Function. Mol Cell Biol *23*, 2762–2777. 10.1128/MCB.23.8.2762-2777.2003.

17. Akil, A., Peng, J., Omrane, M., Gondeau, C., Desterke, C., Marin, M., Tronchère, H., Taveneau, C., Sar, S., Briolotti, P., et al. (2016). Septin 9 induces lipid droplets growth by a phosphatidylinositol-5-phosphate and microtubule-dependent mechanism hijacked by HCV. Nat Commun *7*, 12203. 10.1038/ncomms12203.

18. Zhang, J., Kong, C., Xie, H., McPherson, P.S., Grinstein, S., and Trimble, W.S. (1999). Phosphatidylinositol polyphosphate binding to the mammalian septin H5 is modulated by GTP. Current Biology *9*, 1458–1467. 10.1016/S0960-9822(00)80115-3.

19. Woods, B.L., Cannon, K.S., Vogt, E.J.D., Crutchley, J.M., and Gladfelter, A.S. (2021). Interplay of septin amphipathic helices in sensing membrane-curvature and filament bundling. MBoC *32*, br5. 10.1091/mbc.E20-05-0303.

20. Włoga, D., Strzyżewska-Jówko, I., Gaertig, J., and Jerka-Dziadosz, M. (2008). Septins Stabilize Mitochondria in Tetrahymena thermophila. Eukaryotic Cell *7*, 1373–1386. 10.1128/ec.00085-08.

21. Russell, S.E.H., and Hall, P.A. (2011). Septin genomics: a road less travelled. *392*, 763–767. 10.1515/BC.2011.079.

22. John, C.M., Hite, R.K., Weirich, C.S., Fitzgerald, D.J., Jawhari, H., Faty, M., Schläpfer, D., Kroschewski, R., Winkler, F.K., Walz, T., et al. (2007). The Caenorhabditis elegans septin complex is nonpolar. EMBO J *26*, 3296–3307. 10.1038/sj.emboj.7601775.

23. Nguyen, T.Q., Sawa, H., Okano, H., and White, J.G. (2000). The C. elegans septin genes, unc-59 and unc-61, are required for normal postembryonic cytokineses and morphogenesis but have no essential function in embryogenesis. Journal of Cell Science *113*, 3825–3837. 10.1242/jcs.113.21.3825.

24. Maddox, A.S., Lewellyn, L., Desai, A., and Oegema, K. (2007). Anillin and the Septins Promote Asymmetric Ingression of the Cytokinetic Furrow. Developmental Cell *12*, 827–835. 10.1016/j.devcel.2007.02.018.

25. Perry, J.A., Werner, M.E., Rivenbark, L., and Maddox, A.S. (2023). Caenorhabditis elegans septins contribute to the development and structure of the oogenic germline. Cytoskeleton *80*, 215–227. 10.1002/cm.21763.

26. Finger, F.P., Kopish, K.R., and White, J.G. (2003). A role for septins in cellular and axonal migration in C. elegans. Developmental Biology *261*, 220–234. 10.1016/S0012-1606(03)00296-3.

27. The UniProt Consortium (2023). UniProt: the Universal Protein Knowledgebase in 2023. Nucleic Acids Research *51*, D523–D531. 10.1093/nar/gkac1052.

28. Käll, L., Krogh, A., and Sonnhammer, E.L.L. (2004). A Combined Transmembrane Topology and Signal Peptide Prediction Method. Journal of Molecular Biology *338*, 1027–1036. 10.1016/j.jmb.2004.03.016.

29. Krogh, A., Larsson, B., von Heijne, G., and Sonnhammer, E.L.L. (2001). Predicting transmembrane protein topology with a hidden markov model: application to complete genomes11Edited by F. Cohen. Journal of Molecular Biology *305*, 567–580. 10.1006/jmbi.2000.4315.

30. Letunic, I., and Bork, P. (2021). Interactive Tree Of Life (iTOL) v5: an online tool for phylogenetic tree display and annotation. Nucleic Acids Research *49*, W293–W296. 10.1093/nar/gkab301.

31. Hallgren, J., Tsirigos, K.D., Pedersen, M.D., Armenteros, J.J.A., Marcatili, P., Nielsen, H., Krogh, A., and Winther, O. (2022). DeepTMHMM predicts alpha and beta transmembrane proteins using deep neural networks. Preprint at bioRxiv, 10.1101/2022.04.08.487609 10.1101/2022.04.08.487609.

32. Emms, D.M., and Kelly, S. (2022). SHOOT: phylogenetic gene search and ortholog inference. Genome Biology *23*, 85. 10.1186/s13059-022-02652-8.

33. Edgar, R.C. (2004). MUSCLE: multiple sequence alignment with high accuracy and high throughput. Nucleic Acids Research *32*, 1792–1797. 10.1093/nar/gkh340.

34. Tamura, K., Stecher, G., and Kumar, S. (2021). MEGA11: Molecular Evolutionary Genetics Analysis Version 11. Molecular Biology and Evolution *38*, 3022–3027. 10.1093/molbev/msab120.

35. Brenner, S. (1974). The genetics of Caenorhabditis elegans. Genetics *77*, 71–94. 10.1093/genetics/77.1.71.

36. Dokshin, G.A., Ghanta, K.S., Piscopo, K.M., and Mello, C.C. (2018). Robust Genome Editing with Short Single-Stranded and Long, Partially Single-Stranded DNA Donors in Caenorhabditis elegans. Genetics *210*, 781–787. 10.1534/genetics.118.301532.

37. Benchling https://benchling.com.

38. Madhu, B., Lakdawala, M.F., and Gumienny, T.L. (2022). Small-Scale Extraction of Caenorhabditis elegans Genomic DNA. JoVE, 63716. 10.3791/63716.

39. Schindelin, J., Arganda-Carreras, I., Frise, E., Kaynig, V., Longair, M., Pietzsch, T., Preibisch, S., Rueden, C., Saalfeld, S., Schmid, B., et al. (2012). Fiji: an open-source platform for biological-image analysis. Nat Methods *9*, 676–682. 10.1038/nmeth.2019.

40. Jordan, S.N., Davies, T., Zhuravlev, Y., Dumont, J., Shirasu-Hiza, M., and Canman, J.C. (2016). Cortical PAR polarity proteins promote robust cytokinesis during asymmetric cell division. Journal of Cell Biology *212*, 39–49. 10.1083/jcb.201510063.

41. Lewellyn, L., Carvalho, A., Desai, A., Maddox, A.S., and Oegema, K. (2011). The chromosomal passenger complex and centralspindlin independently contribute to contractile ring assembly. Journal of Cell Biology *193*, 155–169. 10.1083/jcb.201008138.

42. Spiliotis, E.T., and Nakos, K. (2021). Cellular functions of actin- and microtubule-associated septins. Curr Biol *31*, R651–R666. 10.1016/j.cub.2021.03.064.

43. Sulston, J.E., and Horvitz, H.R. (1981). Abnormal cell lineages in mutants of the nematode Caenorhabditis elegans. Developmental Biology *82*, 41–55. 10.1016/0012-1606(81)90427-9.

44. White, J.G., Horvitz, H.R., and Sulston, J.E. (1982). Neurone differentiation in cell lineage mutants of Caenorhabditis elegans. Nature *297*, 584–587. 10.1038/297584a0.

45. Gupta, B.P., Hanna-Rose, W., and Sternberg, P.W. (2018). Morphogenesis of the vulva and the vulval-uterine connection. In WormBook: The Online Review of C. elegans Biology [Internet] (WormBook).

46. Sharma-Kishore, R., White, J.G., Southgate, E., and Podbilewicz, B. (1999). Formation of the vulva in Caenorhabditis elegans: a paradigm for organogenesis. Development *126*, 691–699. 10.1242/dev.126.4.691.

47. Estes, K.A., and Hanna-Rose, W. (2009). The anchor cell initiates dorsal lumen formation during C. elegans vulval tubulogenesis. Developmental Biology *328*, 297–304. 10.1016/j.ydbio.2009.01.034.

48. Schafer, W.R. (2005). Egg-laying. In WormBook: The Online Review of C. elegans Biology [Internet] (WormBook).

49. Cohen, J.D., Sparacio, A.P., Belfi, A.C., Forman-Rubinsky, R., Hall, D.H., Maul-Newby, H., Frand, A.R., and Sundaram, M.V. (2020). A multi-layered and dynamic apical extracellular matrix shapes the vulva lumen in Caenorhabditis elegans. eLife *9*, e57874. 10.7554/eLife.57874.

50. Collins, K.M., Bode, A., Fernandez, R.W., Tanis, J.E., Brewer, J.C., Creamer, M.S., and Koelle, M.R. (2016). Activity of the C. elegans egg-laying behavior circuit is controlled by competing activation and feedback inhibition. eLife *5*, e21126. 10.7554/eLife.21126.

51. Liu, M., and Grigoriev, A. (2004). Protein domains correlate strongly with exons in multiple eukaryotic genomes – evidence of exon shuffling? Trends in Genetics *20*, 399–403. 10.1016/j.tig.2004.06.013.

52. Marsh, J.A., and Teichmann, S.A. (2010). How do proteins gain new domains? Genome Biology *11*, 126. 10.1186/gb-2010-11-7-126.

53. Babushok, D.V., Ostertag, E.M., and Kazazian, H.H. (2007). Current topics in genome evolution: Molecular mechanisms of new gene formation. Cell. Mol. Life Sci. *64*, 542–554. 10.1007/s00018-006-6453-4.

54. Liu, J., Fairn, G.D., Ceccarelli, D.F., Sicheri, F., and Wilde, A. (2012). Cleavage Furrow Organization Requires PIP2-Mediated Recruitment of Anillin. Current Biology *22*, 64–69. 10.1016/j.cub.2011.11.040.

55. Field, C.M., Coughlin, M., Doberstein, S., Marty, T., and Sullivan, W. (2005). Characterization of anillin mutants reveals essential roles in septin localization and plasma membrane integrity. Development *132*, 2849–2860. 10.1242/dev.01843.

56. Panagiotou, T.C., Chen, A., and Wilde, A. (2022). An anillin-CIN85-SEPT9 complex promotes intercellular bridge maturation required for successful cytokinesis. Cell Reports *40*, 111274. 10.1016/j.celrep.2022.111274.

57. Sparacio, A.P., Trojanowski, N.F., Snetselaar, K., Nelson, M.D., and Raizen, D.M. (2020). Teething during sleep: Ultrastructural analysis of pharyngeal muscle and cuticular grinder during the molt in Caenorhabditis elegans. PLoS ONE *15*, e0233059. 10.1371/journal.pone.0233059.

58. Amin, N.D., Zheng, Y.-L., Kesavapany, S., Kanungo, J., Guszczynski, T., Sihag, R.K., Rudrabhatla, P., Albers, W., Grant, P., and Pant, H.C. (2008). Cyclin-Dependent Kinase 5 Phosphorylation of Human Septin SEPT5 (hCDCrel-1) Modulates Exocytosis. J. Neurosci. *28*, 3631–3643. 10.1523/JNEUROSCI.0453-08.2008.

59. Tokhtaeva, E., Capri, J., Marcus, E.A., Whitelegge, J.P., Khuzakhmetova, V., Bukharaeva, E., Deiss-Yehiely, N., Dada, L.A., Sachs, G., Fernandez-Salas, E., et al. (2015). Septin Dynamics Are Essential for Exocytosis. Journal of Biological Chemistry *290*, 5280–5297. 10.1074/jbc.M114.616201.

60. Beites, C.L., Xie, H., Bowser, R., and Trimble, W.S. (1999). The septin CDCrel-1 binds syntaxin and inhibits exocytosis. Nat Neurosci *2*, 434–439. 10.1038/8100.

61. Wasik, A.A., Polianskyte-Prause, Z., Dong, M.-Q., Shaw, A.S., Yates, J.R., Farquhar, M.G., and Lehtonen, S. (2012). Septin 7 forms a complex with CD2AP and nephrin and regulates glucose transporter trafficking. MBoC *23*, 3370–3379. 10.1091/mbc.e11-12-1010.

62. Bartsch, I., Sandrock, K., Lanza, F., Nurden, P., Hainmann, I., Pavlova, A., Greinacher, A., Tacke, U., Barth, M., Busse, A., et al. (2011). Deletion of human GP1BB and SEPT5 is associated with Bernard-Soulier syndrome, platelet secretion defect, polymicrogyria, and developmental delay. Thromb Haemost *106*, 475–483. 10.1160/TH11-05-0305.

63. Dent, J., Kato, K., Peng, X.-R., Martinez, C., Cattaneo, M., Poujol, C., Nurden, P., Nurden, A., Trimble, W.S., and Ware, J. (2002). A prototypic platelet septin and its participation in secretion. Proceedings of the National Academy of Sciences *99*, 3064–3069. 10.1073/pnas.052715199.

FIGURE LEGENDS:

Figure 1: Septins throughout phylogeny are predicted to contain transmembrane domains (TMD). A) A circular cladogram showing the relationship between all septin sequences deposited on UniProt (black) and the sequences containing TMDs (red). Colors on the outside correspond to organismal classes (light purple: nematodes, brown: Arthropods, green: Viridiplantae, yellow: Basidiomycota, orange: Ascomycota, olive green: Aves, light blue: Actinopterygii, peach: Mammals, pink: Bacteria, lilac: SAR). B) Table of TMD-septin containing model organisms detailing septin gene, its homology group, and the TMD location. Colors of classes correspond to those in Figure 1A. C) DeepTMHMM output showing the probability for amino acid residues that correspond to a TMD for *C. elegans* UNC-61. The grey curve indicates residues outside of the membrane, pink curve shows residues corresponding to TMD, and black curve indicates residues in the cytosol. D) Protein alignment of the UNC-61 homologs in *C. elegans* and closely related nematodes; only the first 50 amino acid residues surround the TMD (black box) are shown. Residue colors indicate hydrophobicity; red: hydrophobic, blue : hydrophilic. Neighbor-joining tree (left of protein alignment) depicts the evolutionary relationships among UNC-61 homologs.

Figure 2: *C. elegans* septins are differentially localized. A) Schematic representation of the genomic locus of *unc-61* depicting all three transcripts. Note: *unc-61a* is transcribed from an alternative start (red: ATG). B) Illustration of UNC-61a (pink: TMD, grey: GTP-binding domain, red: SUE, grey: C-terminal extension). Key motifs are also denoted in color (blue: PB1/2, orange: GTPase domains, purple: polyacidic region [PA], green: coiled-coil domain containing the amphipathic helix [AH; light green]). C) Diagrams of the endogenous and exogenous MosSCI loci of UNC-61a::GFP and wrmScarlet::UNC-61b/c animals. D) (top) Schematic diagram of *C. elegans* with pharynx (pink), germline (blue) and vulva (orange). Boxes correspond to location of fluorescent tissues (below). Arrow in UNC-61a::GFP vulva panel: vulval epithelium apical surfaces. Scale bar is 10 µm for the pharynx terminal bulb and vulva and 25 µm for the germline. Images are inverted contrast of the fluorophore annotated.

Figure 3: UNC-61a partially rescues the loss of UNC-61b and UNC-61c. A) Illustration of MosSCI and endogenous loci for control, UNC-61a null (61a Δ), and UNC-61a::GFP/61a Δ animals. B) Brood size measurements of control (yellow) and 61a Δ (salmon) animals (n = 10 animals). B) Percent incidence of post-embryonic phenotypes in control (yellow) and 61a Δ (salmon) animals (n=100 animals). C) Percent incidence of post-embryonic phenotypes in control (grey) and UNC-61a::GFP/61a Δ (teal) animals (n = 100 animals). E) Schematic of MosSCI and endogenous loci for UNC-61a null (61 Δ) and UNC-61a::GFP/ 61 Δ animals. F) Brood size for control, UNC-61a::GFP/61a Δ, 61 Δ, and UNC-61a::GFP/61 Δ animals (n= 10 animals; ****, $p \leq 0.0001$). G) Percent incidence of post-embryonic phenotypes of control (grey), 61 Δ (olive green), UNC-61a::GFP/UNC-61a Δ (teal), and UNC-61a::GFP/ 61 Δ (dark blue) animals (n = 100 animals). Data for control and UNC-61a::GFP/UNC-61a Δ animals is replicated from panel D. H) Body thrashes per minute in control (grey), 61 Δ (olive green), UNC-61a::GFP/UNC-61a Δ (teal), and UNC-61a::GFP/ 61 Δ (dark blue) animals (n = 10-12 animals; ****, $p \leq 0.0001$). I) Distance travelled (mm) by 61 Δ (olive green) and UNC-61a::GFP/ 61 Δ (dark blue) on standard culture plates (n = 30 animals; $p \leq 0.01$). Statistical significance determined by ANOVA corrected with Tukey Multiple Correction test, except in Figure 3G which used t-test. All error bars indicate standard deviation.

Figure 4: UNC-61a TMD is sufficient to drive membrane localization to cellular membranes. A) Top: Illustration of V1::StayGold GFP highlighting the location of the TMD (residues 5-29; pink) within the 71 amino acids included from UNC-61a (grey). Bottom - Inverted contrast images of V1 co-labeled with anti-GM130 (Golgi, magenta), DNA (blue) and actin (phalloidin, white). B) Top – Illustration of V2::StayGold GFP highlighting the location of the TMD (pink) within the 48 amino

acids included from UNC-61a (grey). Bottom - Inverted contrast fluorescent image of V2 in HeLa cells. Arrow denotes nuclear envelope localization. Scale bars = 10 µm.

Figure 5: Loss of UNC-61a TMD disrupts vulval morphology. A) Illustration of UNC-61a and UNC-61a ΔTMD. Colors are as previously described. B) Brood size of control (yellow), 61 Δ (purple), 61a Δ (salmon), and 61a ΔTMD (burgundy) animals (n = 10 animals, ****, $p \leq 0.0001$). C) Percent incidence of post-embryonic phenotypes of control (yellow), 61 Δ (purple), 61a Δ (salmon), and 61a ΔTMD (burgundy) animals (n=100 animals). Data in panel B and panel C for control (yellow) and 61a Δ (salmon) are replicated from Figure 2B and 2C, respectively. D) Top – Schematic of control and 61a ΔTMD vulval epithelium (green), apical surface (black) and surrounding muscles (grey). Bottom – inverted contrast images of lifeAct::GFP (actin) in the tissues described in the schematic. Arrowhead shows connection of muscle to cuticle and arrowhead indicates the apical surface of the vulval epithelium. Scale bar = 20 µm.

Figure 1. Septins throughout phylogeny are predicted to contain transmembrane domains (TMD).

A.

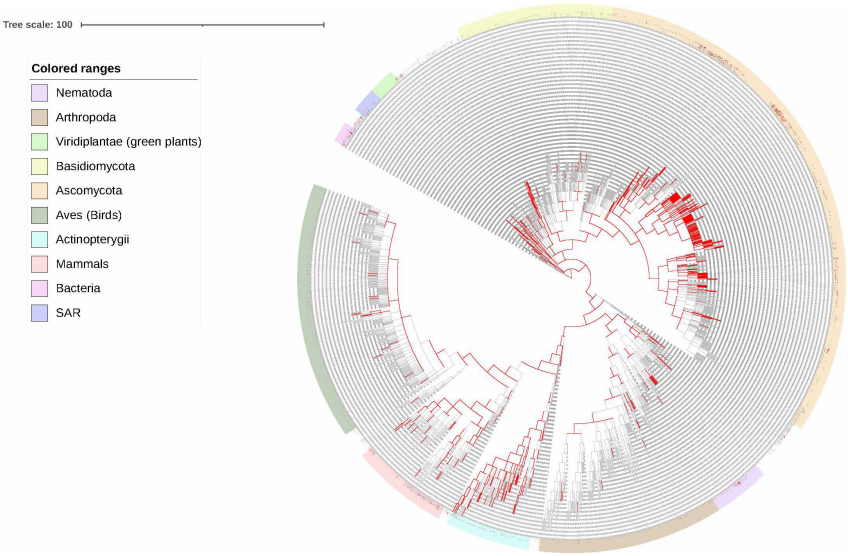

B.

Organism	Class	Septin gene	Septin group	TM Location
S. japonicus	Schizosaccharomycetes	Spn3	3	N-term
C. elegans	Chromadorea	UNC-61	1b	N-term
N. furzeri	Actinopterygii	Septin 8	1b	N-term
X. tropicalis	Amphibia	septin7 septin2 septin11	2b 2b 1b	C-term C-term N-term
C. griseus	Mammalia	Septin-5	2b	C-term

C.

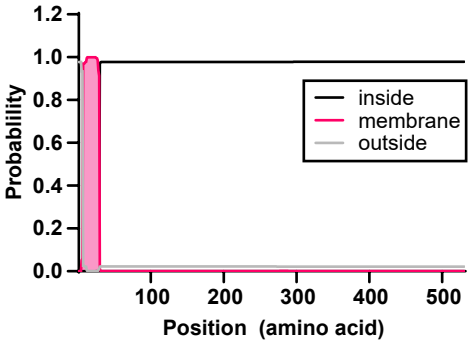

D.

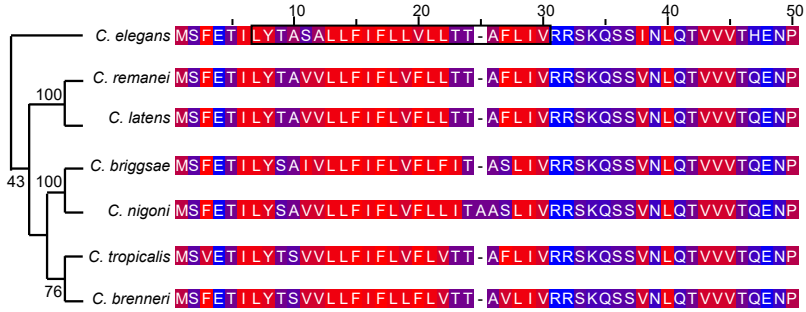

Figure 2. *C. elegans* septins are differentially localized.

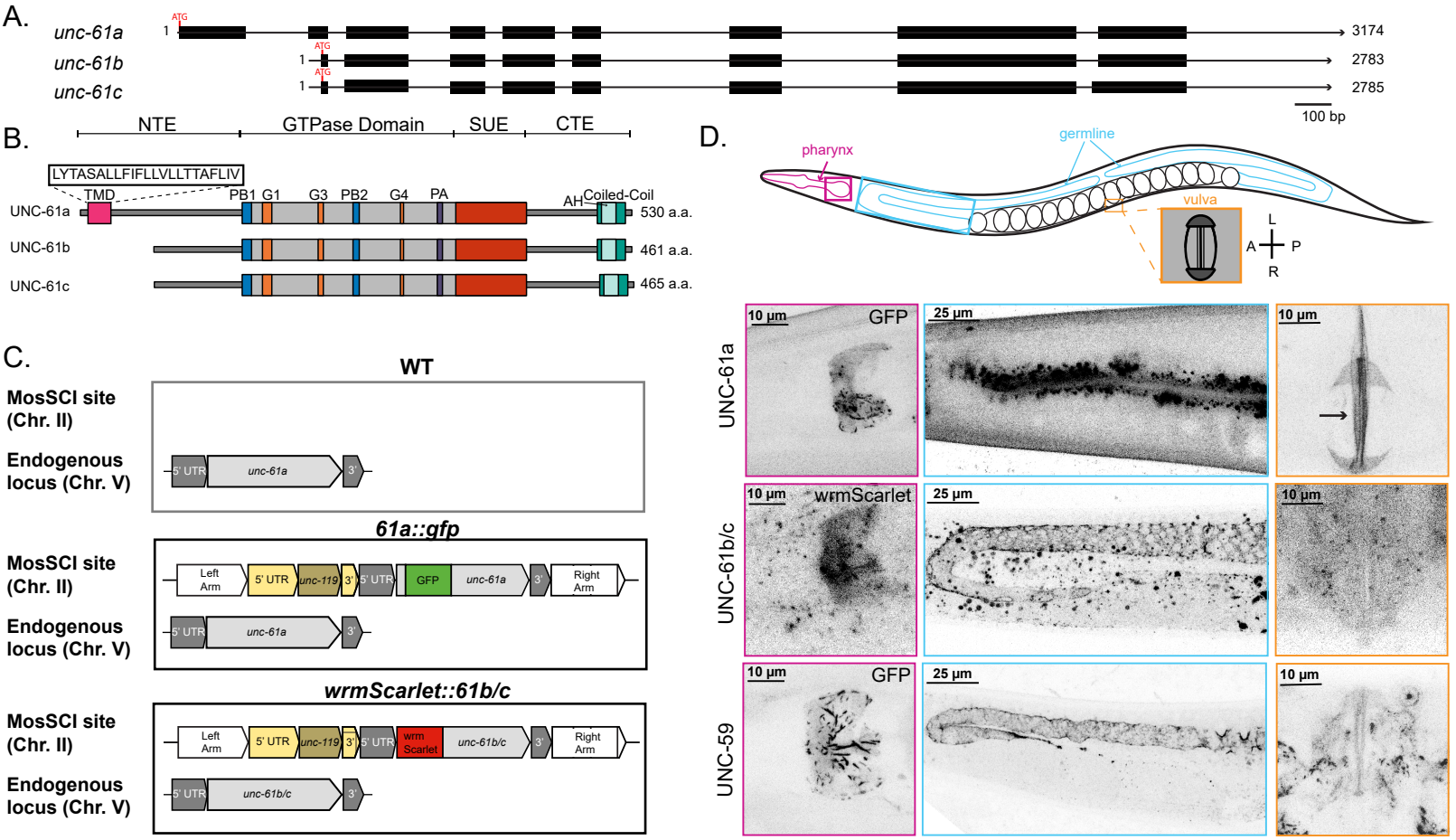

Figure 3: UNC-61a partially rescues the loss of UNC-61b and UNC-61c.

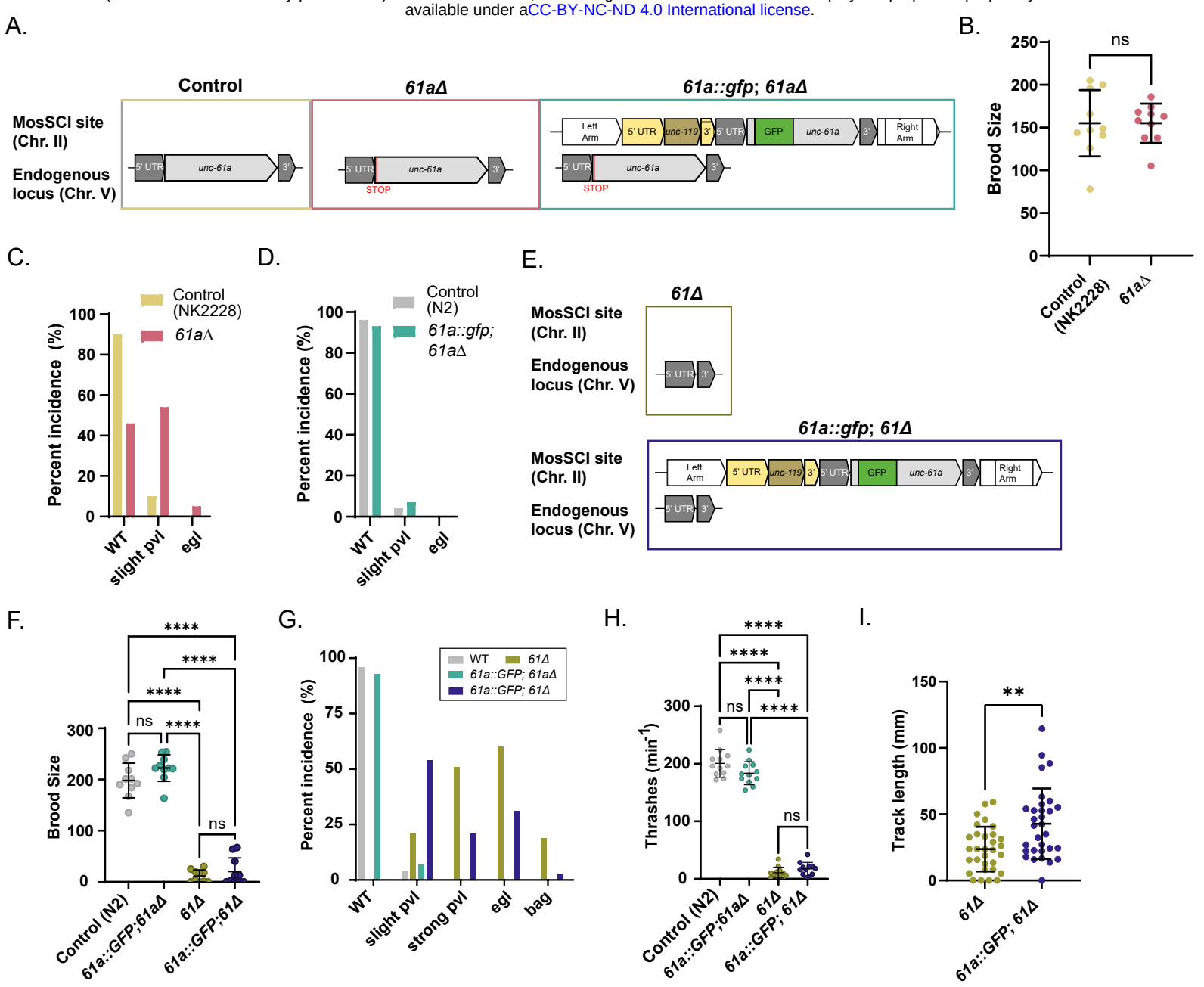

Figure 4: UNC-61a TMD is sufficient to drive membrane localization to cellular membranes.

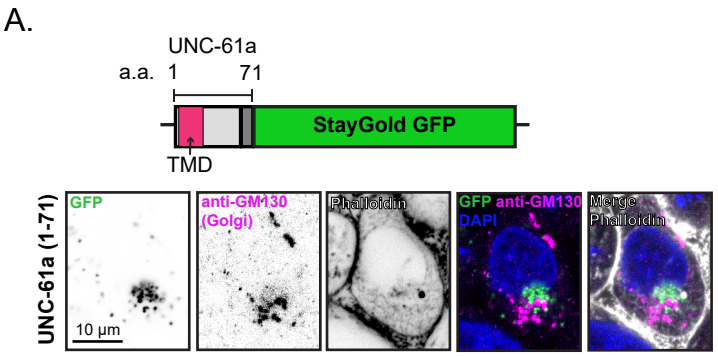

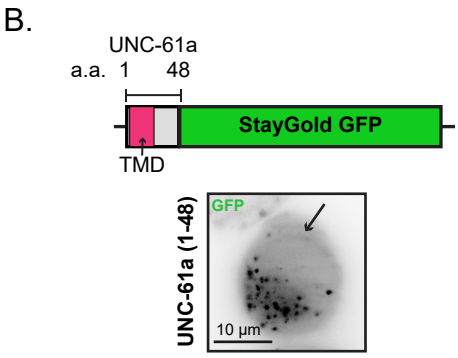

Figure 5: Loss of UNC-61a TMD disrupts vulval morphology.